

# Polarization dynamics and optical selection rules for excitonic transitions in strained quantum wells

Scot A. Hawkins, Martin J. Stevens, and Arthur L. Smirl\*

Laboratory for Photonics and Quantum Electronics 138 IATL, University of Iowa, Iowa City, Iowa 52242

(Received 9 February 2001; published 13 June 2001)

Dual-beam spectral interferometric techniques are used to time resolve the polarization state of the coherent emission from both intentionally and unintentionally strained GaAs/Al<sub>x</sub>Ga<sub>1-x</sub>As multiple quantum wells following irradiation with very weak femtosecond pulses. Any anisotropy in the in-plane strain is shown to result in dramatic oscillations in the intensity, the orientation, and the ellipticity of the coherent emission at the heavy-hole, light-hole beat frequency. This behavior is shown to be the result of replacing the circularly polarized optical selection rules with elliptically polarized selection rules in the uniaxially strained sample. When only the heavy-hole transition is excited with linearly polarized light, these elliptical selection rules lead to a linearly polarized coherent emission that is rotated with respect to the incident orientation. The degree of rotation of the coherent emission as a function of sample orientation is used to quantify the anisotropy in the strain. When the in-plane strain is uniform, no such rotation and no light-hole, heavy-hole beats in the polarization state of the coherent emission are observed.

DOI: 10.1103/PhysRevB.64.035302

PACS number(s): 78.67.De, 71.35.Cc, 78.47.+p, 42.50.Md

## I. INTRODUCTION

Dephasing processes in semiconductors have been studied in detail in recent years.<sup>1</sup> The circularly polarized optical selection rules (CPOSR) for the heavy-hole (*hh*) and light-hole (*lh*) excitonic transitions have played an essential role in the interpretation of many of these experiments. In addition, it is often impossible to avoid introducing stress and strain into the samples used in these experiments during growth and fabrication.<sup>2</sup> For this reason, it is important to understand and to quantify the effects of stress and strain on the optical selection rules. Here, we describe our use of dual-beam spectral interferometric techniques to time resolve the polarization state of the coherent emission induced by a single ultrashort optical pulse in intentionally and unintentionally strained multiple quantum well (MQW) samples. From the dynamics of the polarization state, we determine whether the sample is uniformly or anisotropically strained in the plane of the wells. For the special case of a uniaxially strained sample, we demonstrate that the polarization selection rules are elliptical, as expected, and we extract a numerical value for the difference in the strain tensor elements. That is, we quantify the strain.

## II. EXPERIMENTAL TECHNIQUE

The two samples used in this study are shown schematically in Fig. 1. The first sample [Fig. 1(a)] was prepared using a standard procedure that we (and others) routinely use to prepare our samples for four-wave mixing and other nonlinear optical studies.<sup>3</sup> In this case, no strain and no anisotropy were intentionally introduced. In the second sample [Fig. 1(b)], we intentionally introduced a uniaxial strain. Each sample was prepared from a separate piece of the same wafer, which consists of ten periods of 14-nm-wide GaAs wells alternating with 17-nm-thick Al<sub>0.3</sub>Ga<sub>0.7</sub>As barriers grown on a (001)-oriented GaAs substrate. The first sample was glued to a BK7 glass window, the GaAs substrate was

removed with a selective etch, and an antireflection coating was applied to the top surface. The second sample was processed in a similar manner, except that the sample was bonded to a *b*-cut LiTaO<sub>3</sub> substrate with the *c* axis in the plane of the sample along the [110] axis, as shown in Fig. 1(b). Measurements (to be described below) were then performed on each sample at 80 K. The thermal expansion coefficients<sup>4,5</sup> of GaAs, BK7 and LiTaO<sub>3</sub> are shown in Table I. The thermal expansion coefficients of GaAs and the amorphous BK7 glass are close, but not identical. Consequently, the sample in Fig. 1(a) will be strained, but the strain is expected to be uniform in the plane of the sample. By comparison, the sample in Fig. 1(b) will experience a net compressive uniaxial strain along the *a* axis.<sup>6-8</sup>

The polarization state of the coherent emission induced in each of these samples by a single 172 fs pulse from a mode-locked Ti:sapphire laser was measured using a dual-beam spectral interferometer that we have described previously,<sup>3,9,10</sup> as indicated schematically in Fig. 2. For our purposes, we need only recall that this interferometer allows us to time resolve the amplitude, the phase, and the polarization state of the emitted signal. Also, for the measurements to be described in this paper, the incident pulse was always linearly and *x* polarized, and the sample was rotated by an angle  $\delta$  with respect to the linear polarization of the incident field as shown in Fig. 2(b). The notation that we use for the polarization ellipse of the emitted light is shown in Fig. 2(c). Here,  $\theta_{\text{sig}}$  designates the orientation of the polarization el-

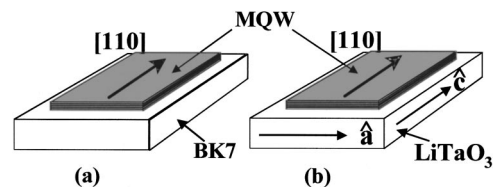


FIG. 1. Schematic drawing of (a) the uniformly strained and (b) the uniaxially strained samples.

TABLE I. The thermal expansion coefficients of the sample and windows at room temperature.

Material	Thermal Expansion Coefficient $\times 10^{-6}/^\circ\text{C}$	Reference
GaAs	6.15	4
BK7 glass	7.1	5
LiTaO <sub>3</sub> (along $a$ )	16.2	4
LiTaO <sub>3</sub> (along $c$ )	4.1	4

lipse and  $\epsilon$  denotes the ellipticity angle, which is determined by the ratio of the minor axis to the major axis.

In general, the emission traveling in the direction of the incident pulse will consist of the transmitted portion of the incident pulse, the first-order coherent emission, and higher-order contributions to the coherent emission. However, the excitation pulses used in the experiments to be reported here had a fluence of  $\sim 20 \text{ nJ/cm}^2$ , which would produce an estimated areal carrier density of  $\sim 10^8 \text{ cm}^{-2}$  (or  $\sim 10^{14} \text{ cm}^{-3}$ ). Consequently, the coherent emission is weak and is dominated by the first-order term. Unless otherwise stated, the laser was tuned so that both  $hh$  and  $lh$  excitonic transitions were excited.

For the measurements on the uniaxial sample, a second LiTaO<sub>3</sub> window was attached to the first and rotated by  $90^\circ$ , so that the optical anisotropy from the first substrate would be compensated by the second. Nevertheless, a small residual anisotropy remained after the insertion of the second substrate. This remaining anisotropy was systematically removed by carefully measuring the Jones matrix<sup>11</sup> of the pair of substrates. The latter was accomplished by measuring the output polarizations after transmission through the pair of substrates for four known input polarizations. The Jones ma-

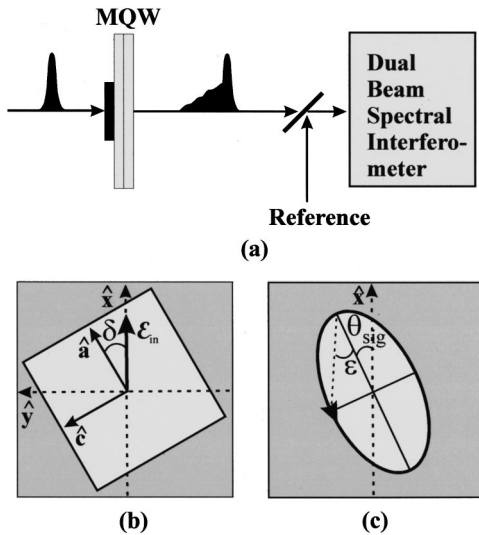


FIG. 2. (a) The experimental geometry for time resolving the polarization state of transmitted and coherently emitted light using dual-beam spectral interferometry. Schematic drawings showing (b) the orientation of the sample relative to the incident  $x$ -polarized radiation and (c) the notation used to describe the polarization ellipse associated with the transmitted and emitted radiation.

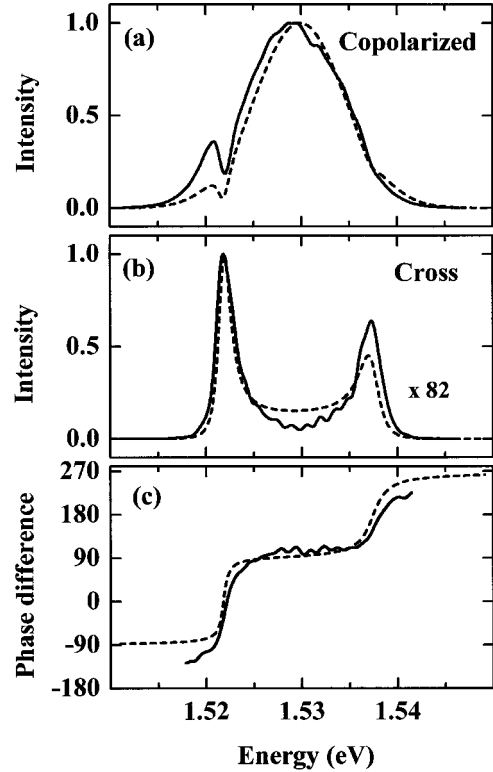


FIG. 3. The spectrally resolved emission from the uniaxially strained sample when the sample was rotated to  $\delta = -45^\circ$  and when both the  $hh$  and  $lh$  excitonic transitions were excited: (a) the  $x$  component  $I_x(\omega)$  and (b) the  $y$  component  $I_y(\omega)$  of the intensity (in arbitrary units) and (c) the spectral phase difference  $\varphi_x(\omega) - \varphi_y(\omega)$  (in degrees) between the  $x$  and  $y$  components of the field. Notice that the  $y$  component of the intensity has been multiplied by a factor of 82 for comparison on the same scale as the  $x$  component. The solid lines are data, and the dashed curves are the results of simulations described in the text.

trix was subsequently calculated from three of the known input polarizations and the corresponding measured output polarizations. As a check, the fourth input polarization was then calculated from the measured output polarization using the calculated matrix. Finally, to ensure consistency, this procedure was repeated for all combinations of the known input polarizations.

### III. RESULTS FOR THE UNIAXIAL SAMPLE

We discuss the results for the uniaxially strained sample first. The measured spectrum of the copolarized (with respect to the  $x$ -polarized incident field) component  $[I_x(\omega)]$  of the emission is shown by the solid line in Fig. 3(a), and the spectrum of the orthogonally polarized component  $[I_y(\omega)]$  is shown in Fig. 3(b). (The dashed lines are the results of simulations to be discussed below.) For these measurements, the sample was oriented such that the strain axis was at  $45^\circ$  with respect to the incident polarization [i.e.,  $\delta = -45^\circ$  in Fig. 2(b)]. The spectrum of the copolarized signal is identical to that of the incident pulse, except for small dips located at the  $hh$  and  $lh$  resonances, indicating that the copolarized signal is dominated by the transmitted portion of the incident

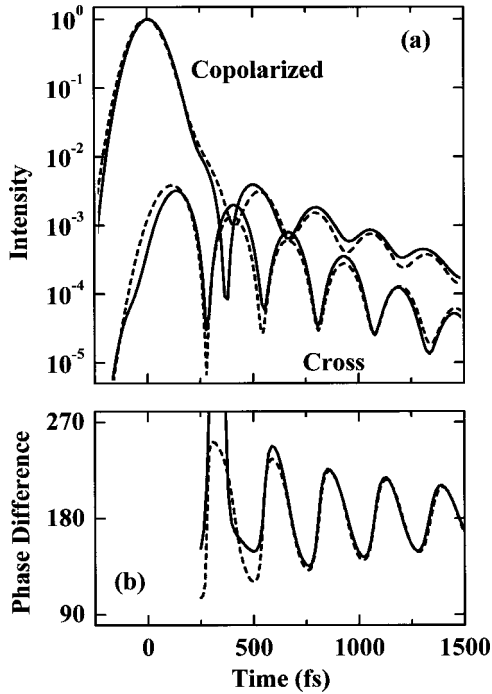


FIG. 4. The temporally resolved emission from the uniaxially strained sample when the sample was rotated to  $\delta = -45^\circ$  and when both the  $hh$  and  $lh$  excitonic transitions were excited: (a) the  $x$  component  $I_x(t)$  and the  $y$  component  $I_y(t)$  of the intensity (upper and lower curves, respectively, in arbitrary units) and (b) the temporal phase difference  $\varphi_x(t) - \varphi_y(t)$  (in degrees) between the  $x$  and  $y$  components of the field. The solid lines are data, and the dashed curves are the results of simulations described in the text.

pulse. By contrast, the cross-polarized spectrum consists predominantly of emission at the  $lh$  and  $hh$  exciton resonances. The very presence of a distinct cross-polarized component to the signal indicates that the sample is anisotropic.<sup>2</sup>

Dual-beam spectral interferometry allows the measurement of the spectral phases as well as the spectral amplitudes [i.e., Figs. 3(a) and 3(b)] of the  $x$  and  $y$  components of the signal. The difference  $[\varphi_x(\omega) - \varphi_y(\omega)]$  between the phases of the copolarized spectrum and the cross polarized spectrum is shown in Fig. 3(c). The copolarized spectral phase,  $\varphi_x(\omega)$ , is approximately constant; therefore, the structure evident in Fig. 3(c) is predominately associated with  $\varphi_y(\omega)$ . Notice that the spectral phase difference has no significance, is difficult to obtain, and therefore, is not shown in spectral regions where there is no measurable contribution from either  $I_x(\omega)$  or  $I_y(\omega)$ .

The temporal signals that are obtained by inverse Fourier transformation of the spectral data in Fig. 3 (including the phase information) are shown in Fig. 4. The time-resolved copolarized component of the signal [upper solid curve in Fig. 4(a)] is dominated at early times by a strong peak corresponding to the transmitted portion of the incident pulse. This initial peak is followed by beats associated with the polarization interference between the linear coherent emissions from the  $hh$  and  $lh$  excitons. By comparison, the cross-polarized component of the signal [lower solid curve in Fig. 4(a)] is much weaker, and it exhibits polarization interfer-

ence beats that are  $180^\circ$  out of phase with those for the parallel component. The temporal phase difference  $[\varphi_x(t) - \varphi_y(t)]$  between the copolarized and cross-polarized fields is shown in Fig. 4(b), and it too exhibits oscillations at the  $hh$ - $lh$  beat frequency. Notice that we show the phase difference only for times after the transmitted pulse has passed. The transmitted portion of the incident pulse is linear and  $x$  polarized, and during the period that it is present, it so dominates the signal that it determines the polarization, making the phase difference between it and the crossed component relatively irrelevant and difficult to determine.

It is interesting to note that the data shown in Figs. 3(a) and 3(b) could have been obtained by performing measurements of the  $x$  and  $y$  components of the signal with a spectrometer, and the upper and lower curves in Fig. 4(a) could have been obtained, for example, by performing a cross-correlation measurement between the signal and a reference pulse in a second harmonic crystal. In fact, when Figs. 3(a), 3(b), and 4(a) are taken together, they provide similar information to that shown in Fig. 3 of Ref. 2. The phase information shown in Figs. 3(c) and 4(b), however, is not provided by these techniques. This information about the relative phases of the copolarized and cross-polarized components is essential if the vectorial dynamics of the coherent first-order emission are to be accurately determined. For example, if one were to assume that the phase difference between the  $x$  and  $y$  components of the field in Fig. 4 is zero, then one would conclude that the emission remains linearly polarized, but that the polarization direction varies in time. However, the time varying amplitudes and phases shown in Fig. 4 suggest a more complicated behavior.

The polarization dynamics are more evident if we plot the data of Fig. 4 in terms of the ellipticity angle  $\varepsilon$  and the azimuthal angle  $\theta_{\text{sig}}$  that determine the polarization ellipse, as we have done in Fig. 5. Clearly both parameters oscillate at the  $lh$ - $hh$  beat frequency. The corresponding temporal behavior of the polarization ellipse for one beat period ( $\sim 265$  fs) is shown in Fig. 6 for selected times. Notice that the orientation of the emission oscillates from  $\sim 0^\circ$  to  $\sim -45^\circ$  and back again each beat period and that the average orientation ( $\sim -25^\circ$ ) is rotated toward the axis of high compressive strain—that is, toward the  $a$  axis. The ellipticity goes from linear to elliptical and then back to linear twice per beat period. Finally, the sense of rotation changes from clockwise (left circular) to counterclockwise (right circular) each period. This behavior can be understood in terms of the  $hh$ - $lh$  mixing associated with the uniaxial strain as described in the next section.

#### IV. THEORETICAL MODEL

The effects of the strain can be readily taken into account by writing the Luttinger Hamiltonian for the valence bands for a compression along the  $[1\bar{1}0]$  direction (our  $a$  axis) and a tension along  $[110]$  (our  $c$  axis).<sup>6,8,12-14</sup> If the strain is treated as a small perturbation and the split-off band is ignored, the strained Hamiltonian for the valence band can be shown to consist of a  $4 \times 4$  matrix composed of two independent  $2 \times 2$  matrices.<sup>6,8,12-14</sup> These matrices can be diago-

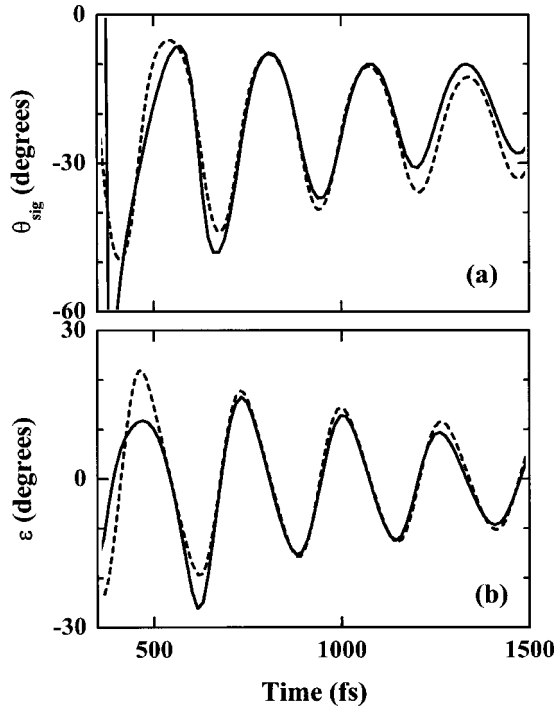


FIG. 5. The time-resolved polarization state for the emission from the uniaxially strained sample when the sample was rotated to  $\delta = -45^\circ$  and when both the  $hh$  and  $lh$  excitonic transitions were excited: (a) the orientation of the polarization ellipse  $\theta_{\text{sig}}(t)$  and (b) its ellipticity angle  $\varepsilon(t)$  in degrees. The solid lines are data, and the dashed curves are the results of simulations described in the text.

nalized to obtain new eigenenergies and eigenfunctions. It is straight forward to show that, at the zone center, the eigenfunctions of the strained Hamiltonian for the valence band are of the form:

$$|hh\rangle_{\pm} = a_1 \left| \frac{3}{2}, \pm \frac{3}{2} \right\rangle + a_2 \left| \frac{3}{2}, \mp \frac{1}{2} \right\rangle, \quad (1)$$

$$|lh\rangle_{\pm} = -a_2 \left| \frac{3}{2}, \pm \frac{3}{2} \right\rangle + a_1 \left| \frac{3}{2}, \mp \frac{1}{2} \right\rangle, \quad (2)$$

where  $|3/2, \pm 3/2\rangle$  and  $|3/2, \pm 1/2\rangle$  denote the doubly degenerate  $hh$  and  $lh$  basis states of the unstrained Hamiltonian,

$$a_1 = \frac{1}{\sqrt{2}} (1 + \sqrt{1 - R^2})^{1/2} \quad (3)$$

and

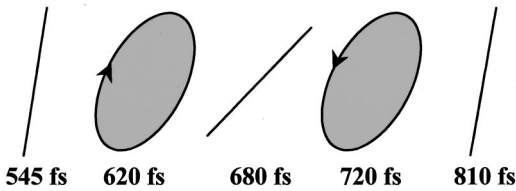


FIG. 6. Sketches of the polarization ellipse at selected times during a single oscillation period corresponding to the data in Fig. 5.

$$a_2 = \frac{1}{\sqrt{2}} (1 - \sqrt{1 - R^2})^{1/2}, \quad (4)$$

and where for this strain configuration,  $R$  is defined as the ratio

$$R = \frac{d(\varepsilon_a - \varepsilon_c)}{\Delta}, \quad (5)$$

where  $\varepsilon_a$  and  $\varepsilon_c$  are the compressive and tensile strains along the  $a$  and  $c$  axes, respectively,  $d$  is the deformation potential appropriate for rhombohedral symmetry, and  $\Delta$  is the  $hh$ - $lh$  hole splitting under these deformations. The conduction-band states remain parabolic and are denoted here as

$$|e\rangle_{\pm} = \left| \frac{1}{2}, \pm \frac{1}{2} \right\rangle. \quad (6)$$

In the absence of strain or for a uniform in-plane strain, the valence-to-conduction band optical transitions can be shown to obey the CPOSR. For an interaction Hamiltonian of the form  $-\vec{\mu} \cdot \mathbf{E}$  (where  $\mathbf{E}$  denotes the incident field), the nonzero dipole matrix coupling elements are given by

$$\mu_{\text{eh}}^{(+)} = {}_+ \langle e | \mu | hh \rangle_+ = \left\langle \frac{1}{2}, \frac{1}{2} \left| \mu \right| \frac{3}{2}, \frac{3}{2} \right\rangle = \mu_{\text{eh}}(\hat{\sigma}_-)^*, \quad (7)$$

$$\mu_{\text{el}}^{(+)} = {}_+ \langle e | \mu | lh \rangle_+ = \left\langle \frac{1}{2}, \frac{1}{2} \left| \mu \right| \frac{3}{2}, -\frac{1}{2} \right\rangle = \mu_{\text{el}}(\hat{\sigma}_+)^*, \quad (8)$$

$$\mu_{\text{eh}}^{(-)} = {}_- \langle e | \mu | hh \rangle_- = \left\langle \frac{1}{2}, -\frac{1}{2} \left| \mu \right| \frac{3}{2}, -\frac{3}{2} \right\rangle = \mu_{\text{eh}}(\hat{\sigma}_+)^*, \quad (9)$$

$$\mu_{\text{el}}^{(-)} = {}_- \langle e | \mu | lh \rangle_- = \left\langle \frac{1}{2}, -\frac{1}{2} \left| \mu \right| \frac{3}{2}, \frac{1}{2} \right\rangle = \mu_{\text{el}}(\hat{\sigma}_-)^*, \quad (10)$$

where  $\hat{\sigma}_+ = (\hat{\mathbf{a}} + i\hat{\mathbf{c}})/\sqrt{2}$  and  $\hat{\sigma}_- = (\hat{\mathbf{a}} - i\hat{\mathbf{c}})/\sqrt{2}$  are the unit vectors for right and left circularly polarized light, respectively, referenced to the strain axes and where  $\mu_{\text{eh}}$  and  $\mu_{\text{el}}$  are the  $hh$  and  $lh$  matrix elements for the unstrained system, respectively.

In the presence of an anisotropic in-plane strain, however, one can use Eqs. (1) and (2) to show that the mixing of the  $lh$  and  $hh$  valence bands leads to elliptical coupling between the new eigenstates. In this case, the elliptically polarized optical selection rules (EPOSR) are given by

$$\mu_{\text{eh}}^{(+)} = {}_+ \langle e | \mu | hh \rangle_+ = \mu_{\text{eh}} \left[ a_1 (\hat{\sigma}_-)^* + \frac{a_2}{\sqrt{3}} (\hat{\sigma}_+)^* \right], \quad (11)$$

$$\mu_{\text{el}}^{(+)} = {}_+ \langle e | \mu | lh \rangle_+ = \mu_{\text{el}} [-\sqrt{3} a_2 (\hat{\sigma}_-)^* + a_1 (\hat{\sigma}_+)^*], \quad (12)$$

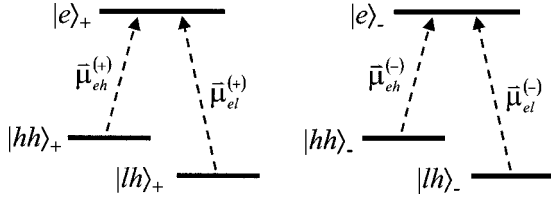


FIG. 7. The energy-level diagram used to model the  $hh$  and  $lh$  excitonic transitions. The matrix elements and eigenstates are given in the text.

$$\mu_{eh}^{(-)} = -\langle e | \boldsymbol{\mu} | hh \rangle_- = \mu_{eh} \left[ a_1 (\hat{\sigma}_+)^* + \frac{a_2}{\sqrt{3}} (\hat{\sigma}_-)^* \right], \quad (13)$$

$$\mu_{el}^{(-)} = -\langle e | \boldsymbol{\mu} | lh \rangle_- = \mu_{el} [-\sqrt{3} a_2 (\hat{\sigma}_+)^* + a_1 (\hat{\sigma}_-)^*]. \quad (14)$$

Notice that in the absence of anisotropic strain,  $a_2=0$  and  $a_1=1$ , and the EPOSr reduce to the CPOSr given by Eqs. (7)–(10). That is, the  $|hh\rangle_+$  valence state is coupled to the  $|e\rangle_+$  conduction state by right circularly polarized light, and the  $|lh\rangle_+$  valence state is coupled to the same  $|e\rangle_+$  conduction state by left circular light. By comparison, the  $|hh\rangle_-$  valence state is coupled to the  $|e\rangle_-$  conduction state by left circularly polarized light, and the  $|lh\rangle_-$  valence state is coupled to the  $|e\rangle_-$  conduction state by right circular light. In this case, there is no preferred direction for absorption. In the presence of uniaxial strain, the  $lh$  and  $hh$  wave functions are mixed so that the selection rules become elliptical, with the major axis of the  $hh$  ellipse aligned along the compressive strain axis (i.e., parallel to  $\hat{\mathbf{a}}$ ) and the  $lh$  ellipse perpendicular to this axis (i.e., parallel to  $\hat{\mathbf{c}}$ ). In other words, the  $hh$  matrix element is increased along the compression axis and decreased along the tension axis. In contrast, the  $lh$  transition strength is increased along the tension axis and decreased along the compression axis. Oscillator strength is conserved through  $|a_1|^2 + |a_2|^2 = 1$ .

When the incident radiation is resonant with the excitonic transitions, the linear absorption of this system is most easily calculated by representing the  $hh$  and  $lh$  excitonic transitions by two independent three-level systems obeying the selection rules given by Eqs. (11)–(14) as depicted schematically in Fig. 7. A first-order perturbative solution to the density matrix equations for these two systems in response to a delta function excitation pulse gives

$$\begin{pmatrix} \mathcal{P}_{co} \\ \mathcal{P}_{cross} \end{pmatrix} \propto \left( \frac{i\mu_{eh}^2}{\hbar} \right) \mathcal{E} \theta(t) e^{-\gamma t} \left\{ \left[ (a_1^2 + a_2^2/3) + a_2^2 + a_1^2/3 \right] e^{-i\Omega t} \begin{pmatrix} \hat{\mathbf{x}} \\ 0\hat{\mathbf{y}} \end{pmatrix} + \frac{2a_1a_2}{\sqrt{3}} [1 - e^{-i\Omega t}] \times \begin{pmatrix} \cos 2\delta\hat{\mathbf{x}} \\ \sin 2\delta\hat{\mathbf{y}} \end{pmatrix} \right\}, \quad (15)$$

for the copolarized,  $\mathcal{P}_{co}$ , and cross polarized,  $\mathcal{P}_{cross}$  components of the emission, where  $\gamma$  is the exciton dephasing rate

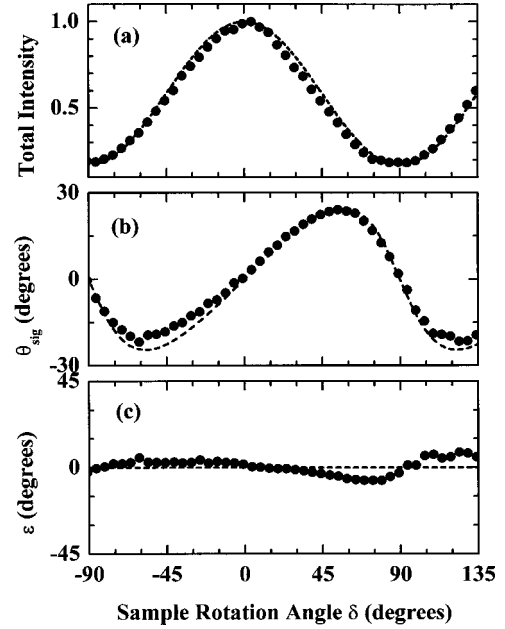


FIG. 8. The gated, time-averaged polarization state for the emission from the uniaxially strained sample as a function of sample orientation when only the  $hh$  excitonic transition was excited: (a) the total intensity (in arbitrary, but relative units), (b) the orientation of the polarization ellipse  $\theta_{sig}$ , and (c) the ellipticity angle  $\epsilon$ . The solid circles are data, and the dashed curves are the results of simulations described in the text.

(for the moment, assumed to be the same for both  $hh$  and  $lh$ ),  $\Omega$  is the  $hh$ - $lh$  splitting,  $\mathcal{E}$  is the incident field amplitude,  $\theta(t)$  is the Heaviside step function, and  $\delta$  is the angle between the compressive strain axis and the incident linear polarization. We will use this expression to guide our qualitative discussions in the following sections.

## V. EXTRACTION OF STRAIN PARAMETERS

The polarization state of the coherent emission as given by Eq. (15) clearly depends upon sample orientation, and we can use this orientational dependence to quantify the strain. For these measurements, the laser was tuned so that we excited only the  $hh$  transitions. Note that when only the  $hh$  excitons are excited, Eq. (15) is simplified by the elimination of all terms multiplied by  $\exp(-i\Omega t)$ :

$$\begin{pmatrix} \mathcal{P}_{co} \\ \mathcal{P}_{cross} \end{pmatrix} \propto \left( \frac{i\mu_{eh}^2}{\hbar} \right) \mathcal{E} \theta(t) e^{-\gamma t} \left\{ (a_1^2 + a_2^2/3) \begin{pmatrix} \hat{\mathbf{x}} \\ 0\hat{\mathbf{y}} \end{pmatrix} + \frac{2a_1a_2}{\sqrt{3}} \begin{pmatrix} \cos 2\delta\hat{\mathbf{x}} \\ \sin 2\delta\hat{\mathbf{y}} \end{pmatrix} \right\}. \quad (16)$$

The *time-integrated* intensity and the *time-averaged* orientation and ellipticity of the emitted first-order field as a function of the orientation of the sample are shown in Fig. 8 when only the  $hh$  is excited. These time-averaged parameters were obtained by gating the time-resolved emission to remove the contributions of the transmitted pulse in the following way. We first time resolved the  $x$  and  $y$  components of

the intensity and the phase, as described in our discussions surrounding Figs. 3 and 4. For convenience, we then expressed this data in terms of the time-resolved Stokes parameters,<sup>11</sup> and we numerically integrated the time-resolved Stokes parameters beginning at a time of roughly 400 fs after the pump pulse. Finally, we converted the time-integrated Stokes parameters to time-averaged values for the ellipticity and the orientation. This procedure was repeated for each sample orientation. In this way, we were able to eliminate the effects of the transmitted pump pulse (and the reflection from the second substrate that we describe below) and were able to average over the first-order emission only.

Several features in Fig. 8 are worth noting. First, in agreement with Eq. 16, the emission is in general rotated, but linearly polarized (i.e.,  $\varepsilon \equiv 0$ ) for all sample orientations. The total emission is strongest when the incident polarization is parallel to the compressive strain axis ( $\delta=0$ ), and it decreases with angle until the polarization is along the tensile strain axes ( $\delta=90^\circ$ ). When the incident polarization is along one of these axes, there is no cross-polarized component, and the emission is  $x$  polarized. However, when the incident polarization is not oriented along either of these axes, the emission is rotated towards the compressive strain axis.

The dashed curves in Fig. 8 are the results of simulations based on Eq. (16) and on the elliptical selection rules given by Eqs. (11)–(14). From such fits, we are able to extract a value of  $a_2=0.353\pm 0.004$ . Using this value for  $a_2$  in Eqs. (4) and (5), we can estimate the net compressive strain to be  $\varepsilon_a - \varepsilon_c = -2.3 \times 10^{-3}$ . In making this estimate, we have used the measured  $hh$ - $lh$  splitting of  $\Delta=15.6$  meV and taken  $d = -4.55$  eV.<sup>15</sup>

Numerical simulations using finite pulses (172 fs, full width at half maximum of the intensity), the elliptical selection rules given by Eqs. (11)–(14), and  $a_2=0.353$  are shown by the dashed curves in Figs. 3–6. For these simulations, we assumed that the pulses were tuned 8.1 meV above the  $hh$  transition, in agreement with the experimental detuning. Clearly, all of the key features in the data are accurately reproduced by these simulations. One exception is the disagreement between simulation and experiment near 260 fs, which is particularly evident in Fig. 4. The anomalous experimental behavior at this time has been identified as a reflection from the interface between the crossed LiTaO<sub>3</sub> windows, and it has the same polarization as the incident pulse. This reflection makes it difficult to extract the correct intensity and phase of the copolarized emission in this temporal region. One final remark concerning the simulations is that, in order to correctly account for the decay of the oscillations in  $\varepsilon$  and  $\theta_{\text{sig}}$  (see Fig. 5), it was necessary to take the dephasing rate for the  $lh$  to be slightly larger than the  $hh$ . We offer no justification for this ansatz.

## VI. RESULTS FOR THE UNIFORMLY STRAINED SAMPLE

Finally, in Fig. 9(a), we show the emission that is copolarized and cross polarized to the incident field as a function of time for the conventionally prepared sample mounted on

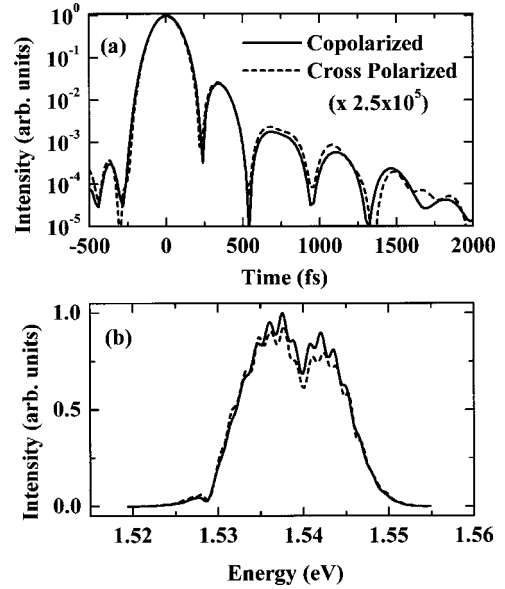


FIG. 9. The (a) temporally resolved and (b) spectrally resolved  $x$  component (solid) and  $y$  component (dashed) of the emitted intensity from the uniformly strained sample when both the  $hh$  and  $lh$  excitonic transitions were excited. Notice that the  $y$  component of the intensity has been multiplied by a factor of  $2.5 \times 10^5$  for comparison on the same scale as the  $x$  component. This result was independent of sample orientation.

the amorphous glass substrate when both  $hh$  and  $lh$  are excited. The spectra for the parallel and orthogonal intensities are also shown [Fig. 9(b)]. As in Fig. 4, the copolarized component of the time-resolved signal is dominated by a peak corresponding to the transmitted portion of the incident pulse, and this peak is followed by beats associated with the polarization interference between the linear coherent emission from the  $hh$  and  $lh$  excitons. In contrast to the uniaxial measurements, however, the orthogonal signal and spectrum are in every respect identical to the parallel signals, except that they are reduced in magnitude by  $4 \times 10^{-6}$ , which is equal to the measured leakage of our analyzer. Thus, to within the accuracy of our measurements, the light from this sample is linearly and  $x$  polarized. This result is independent of sample orientation. This confirms the validity of the CPOSR and confirms that the processing used to mount the sample has introduced no measurable anisotropy.

## VII. SUMMARY AND CONCLUSIONS

Time resolving the polarization state of the coherent emission induced by weak ultrashort pulses from these two MQW samples has allowed us to characterize the in-plane anisotropic strain present in the samples. Our intentionally uniaxially strained sample, mounted on LiTaO<sub>3</sub>, shows clear evidence of anisotropy. From measurements of the time-integrated polarization state of the  $hh$  emission as a function of sample orientation, the  $hh$ - $lh$  valence-band mixing parameters have been determined. By comparison, our conventional sample mounted on BK7 glass, shows no sign of an-

isotropic strain, validating the use of the circular polarization optical selection rules in describing the coherent emission from this sample. Finally, as a note of caution, it should be pointed out that, in contrast to our results using amorphous substrates and our mounting procedures, another group<sup>2</sup> has investigated samples glued to *c*-cut sapphire substrates and has found evidence of a small, but detectable, strain-induced anisotropy. While these effects<sup>2</sup> were small, nevertheless, the validity of the CPOSR may depend upon the manner in

which the sample is prepared and mounted and upon the sensitivity of the measurements to any anisotropy present.

#### ACKNOWLEDGMENTS

The authors gratefully acknowledge numerous insightful conversations with Rolf Binder and Eric Gansen. This research was supported in part by the U.S. Army Research Office and the Office of Naval Research.

\*Fax: 319-335-3462; Email address: art-smirl@uiowa.edu

<sup>1</sup>J. Shah, *Ultrafast Spectroscopy of Semiconductors and Semiconductor Nanostructures*, 2nd ed. (Springer-Verlag, New York, 1999) and references therein.

<sup>2</sup>N. H. Bonadeo, D. G. Steel, and R. Merlin, *Phys. Rev. B* **60**, 8970 (1999).

<sup>3</sup>A. L. Smirl, in *Ultrafast Phenomena in Semiconductors*, edited by K.-T. Tsen (Springer-Verlag, New York, 2001), pp. 443–507, and references therein.

<sup>4</sup>Y. Lu, H. C. Kuo, H. Shen, M. Taysing-Lara, M. Wraback, J. Pamulapati, M. Dutta, J. Kosinski, and R. Sacks, in *Electronic and Photonic Device Fabrication and Performance*, edited by K. J. Jones, S. J. Pearton, and H. Kanber, Mater. Res. Soc. Symp. Proc. Symposia Proceedings No. 300 (Materials Research Society, Pittsburgh, 1993), p. 537.

<sup>5</sup>Melles Griot Catalog 2000.

<sup>6</sup>H. Shen, M. Wraback, J. Pamulapati, P. G. Newman, M. Dutta,

Y. Lu, and H. C. Kuo, *Phys. Rev. B* **47**, 13 933 (1993).

<sup>7</sup>M. F. Huang, E. Garmire, A. Partovi, and M. Hong, *Appl. Phys. Lett.* **66**, 736 (1995).

<sup>8</sup>M.-F. Huang, E. Garmire, and Y.-K. Kuo, *Jpn. J. Appl. Phys., Part 1* **39**, 1776 (2000).

<sup>9</sup>W. J. Walecki, D. N. Fittinghoff, A. L. Smirl, and R. Trebino, *Opt. Lett.* **22**, 81 (1997).

<sup>10</sup>A. L. Smirl, X. Chen, and O. Buccafusca, *IEEE J. Quantum Electron.* **35**, 523 (1999).

<sup>11</sup>R. M. A. Azzam and N. M. Bashara, *Ellipsometry and Polarized Light* (North-Holland, Amsterdam, 1977), Chap. 3.

<sup>12</sup>F. H. Pollak, in *Strained-Layer Superlattices: Physics, Semiconductors and Semimetals*, Vol. 32, edited by T. T. Pearsall (Academic, New York, 1990), pp. 17–53.

<sup>13</sup>F. H. Pollak and M. Cardona, *Phys. Rev.* **172**, 816 (1968).

<sup>14</sup>R. Binder, *Phys. Rev. Lett.* **78**, 4466 (1997).

<sup>15</sup>S. Adachi, *J. Appl. Phys.* **53**, 8775 (1985).